PROTEINS: Structure, Function, and Genetics 3:32–52 (1988)

Energetics of Charge–Charge Interactions in Proteins

Michael K. Gilson and Barry H. Honig
Department of Biochemistry and Molecular Biophysics, Columbia University, New York, New York 10032

ABSTRACT **Electrostatic interactions between pairs of atoms in proteins are calculated with a model based on the linearized Poisson-Boltzmann equation. The equation is solved accurately by a method that takes into account the detailed shape of the protein. This paper presents applications to several systems. Experimental data for the interaction of ionized residues with an active site histidine in subtilisin BPN′ allow the model to be tested, using various assumptions for the electrical properties of the protein and solvent. The electrostatic stabilization of the active site thiolate of rhodanese is analyzed, with attention to the influence of α-helices. Finally, relationships between electrostatic potential and charge–charge distance are reported for large and small globular proteins. The above results are compared with those of simpler electrostatic models, including Coulomb's law with both a distance-dependent dielectric constant ($\epsilon = R$) and a fixed dielectric constant ($\epsilon = 2$), and Tanford-Kirkwood theory. The primary conclusions are as follows: 1) The Poisson-Boltzmann model agrees with the subtilisin data over a range of ionic strengths; 2) two α-helices generate a large potential in the active site of rhodanese; 3) $\epsilon = R$ overestimates weak electrostatic interactions but yields relatively good results for strong ones; 4) Tanford-Kirkwood theory is a useful approximation to detailed solutions of the linearized Poisson-Boltzmann equation in globular proteins; and 5) the modified Tanford-Kirkwood theory overscreens the measured electrostatic interactions in subtilisin.**

Key words: alpha-helix, distance-dependent, finite-difference method, Poisson-Boltzmann equation, protein electrostatics, rhodanese, solvent effects, subtilisin, Tanford-Kirkwood theory

INTRODUCTION

Electrostatic interactions are believed to play key roles in a range of biologically important protein functions.[1–4] Examples include specific binding, voltage gating of membrane channels, enzyme catalysis, and the determination of spectral properties of biological pigments.[5,6] Electrostatic interactions are also of crucial importance in protein folding, as evidenced by the pH dependence of protein stability.[7]

The calculation of charge–charge interactions, although of obvious importance, presents a serious challenge. In particular, simulations that include a microscopic description of solvent molecules demand very large amounts of computer time when dielectric properties are important, especially if the solvent contains an electrolyte. Moreover, it is still not clear how well current models of this type reproduce the dielectric properties of liquid water.[8,9] It is therefore of interest to explore the range of applicability of continuum models for electrostatic interactions, since these appear to incorporate the essential electrical properties of the systems and are more computationally tractable.

Continuum models[10] treat the protein and the solvent as homogeneous dielectric media. In cases in which the three-dimensional structure of the protein has been solved, the coordinates of its charged atoms (ionized groups and partially charged atoms), as well as its overall shape, can be included in detail. Since the protein is a low dielectric medium,[11] and the solvent is a high dielectric medium, the protein surface constitutes a dielectric interface. As a consequence, Coulomb's law, which holds only for homogeneous, isotropic media, does not apply in most protein-solvent systems. The Poisson-Boltzmann equation—the basis of the Debye-Huckel and Gouy-Chapmann theories—offers a natural basis for treating such systems, since it allows the dielectric constant and ionic strength to vary through space. Because the Poisson-Boltzmann equation cannot be solved analytically for the shapes of actual proteins, most of its applications to protein electrostatics to date have dealt with a hypothetical spherical molecule,[3,12–16] for which analytic solutions were obtained by Kirkwood.[17] In some of these applications, the deviation of protein shape from sphericity has been treated by adjusting the assumed depths of charges below the sphere's surface,[12] or by incorporating an additional factor whose magnitude diminishes with increasing solvent exposure of a titratable group[3] (see "Materials and Methods").

Recently, however, numerical techniques that can account for the detailed shape of a dielectric boundary, have been introduced to solve the Poisson-Boltzmann equation for problems in protein electrostatics.[18–22] These methods have so far been applied in analyzing the electrostatic field around Klenow fragment of DNA polymerase I,[23] the diffusion of

Received July 23, 1987; accepted October 14, 1987.

Address reprint requests to Dr. Barry H. Honig, Department of Biochemistry and Molecular Biophysics, Columbia University, 630 West 168th Street, New York, NY 10032.

substrate to the active site of Cu,Zn superoxide dismutase,[24,25] active site potentials produced by α-helices in phosphoglycerate mutase,[21,26] the interaction of α-helices in a hypothetical spherical protein[20] the control of the redox potential of cytochrome c_{551},[27] and the interaction of charged residues with the active site histidine of subtilisin BPN.[28,60]

The studies on subtilisin BPN′, based on experiments by Fersht and coworkers,[29,30] provide an excellent test for models of protein electrostatics. In the present study we examine the consequences of various assumptions for side chain conformations, the dielectric constant of surface water, the protein dielectric constant (ϵ_p), and the Stern layer thickness (r_S) (see below) on the level of agreement with experiment for the detailed Poisson-Boltzmann model. These comparisons with experiment test the range of validity of the Poisson-Boltzmann equation. This has not been well explored in the past, in part because the equation could not be solved for systems of complicated shape.

We also describe a straightforward method of dissecting the contributions of various elements of protein structure to the potential at a given location, within the context of the linearized Poisson-Boltzmann model for protein electrostatics. For the case of the catalytic cysteine in the enzyme rhodanese, we find that the potential at the cysteine results largely from a long-range interaction with two α-helices, in accord with the suggestions of Hol and coworkers[1,31,32] and of Wada.[33] The part of the potential at the cysteine that is not produced by the helices results primarily from short-range interactions with dipolar groups.

In order to ascertain the range of electrostatic interactions in a more general way, we examine the relationship between electrostatic potential and charge–charge distance in the proteins bovine pancreatic trypsin inhibitor (BPTI) and rhodanese. This analysis may be useful in refining the treatment of electrostatic interactions in molecular mechanics simulations.

The three studies just described (subtilisin pK shifts, rhodanese active site potential, general characterization of charge–charge interactions) are also used as the basis for comparisons of the Poisson-Boltzmann model with several simpler electrostatic models in common use. These include the Tanford-Kirkwood model,[15] the Modified Tanford-Kirkwood model,[3] Coulomb's law using the distance dependent dielectric ($\epsilon = R$) model, and Coulomb's law with $\epsilon = 2$.

MATERIALS AND METHODS

Solution of the Linearized Poisson-Boltzmann Equation

We used the macromolecular electrostatics package DelPhi[18] to solve the linearized Poisson-Boltzmann equation. A collection of FORTRAN programs goes from a protein structure in Brookhaven Protein Data Bank format to a set of three-dimensional arrays used in the finite difference algorithm. A "focusing" method is used to improve the boundary conditions, and rotational averaging[18] reduces the errors associated with the grid representation of the electrostatic system. The finite-difference iterations were carried out on an ST-100 array processor. The solutions should be accurate to within about 10%.

Rotational averaging was not used in all the calculations presented here, however. Since averaging the subtilisin results over six rotations produced less than 5% change in the final results for several test cases, only a single orientation was used for the remaining subtilisin computations.

Application to Proteins (Subtilisin, BPTI, and Rhodanese)

Choice of dielectric constant

As already discussed,[2,10,11] the appropriate dielectric constant, ϵ_p, to use for the protein interior depends on the particular application. If the electrostatic field produced by a protein in the state in which its structure has been determined is to be calculated, then the high-frequency dielectric constant, ϵ_∞, should be used for ϵ_p. However, in systems where the charge distribution changes, as in titration of an ionizable group, dipolar reorientation should be accounted for by using an increased dielectric constant. The high-frequency dielectric constant of a protein, including only electronic polarizability, is probably about 2. Including dipolar reorientation yields protein dielectric constants of about 2–4.[11] Given the uncertainty in the value of ϵ_p, we have generally used the lower value, which we believe to be most accurate, but we have also explored the results of varying this parameter in most of the following studies.

Dissection of electrostatic energies

The interaction of one element of protein structure with all other parts of the protein can readily be analyzed by the following method. The linearized Poisson-Boltzmann equation is solved with only the element of interest considered to be charged. (This part of the protein is called the "source.") This yields an electrostatic potential everywhere in the protein, which can be used to calculate the potential at each charged atom other than the source. The source's energy of interaction with any other part of the protein is

$$G^0 = \sum_{i=1}^{N} q_i \phi_i \qquad (1)$$

where q_i is the charge of atom i, ϕ_i is the potential at atom i that is due to the source, and N is the number of atoms making up the other part of the protein. (This formula is invalid for the full nonlinear Poisson-Boltzmann equation.)

As an example, the calculations presented here for the rhodanese active site are all based on one Poisson-Boltzmann calculation, in which only the sulfur of Cys 247 (the source) was considered charged (−1). This yielded the potential at every charged atom in the protein. Simply selecting a subset of atoms and summing $q_i\phi_i$ for them yields their interaction energy with the thiolate form of the cysteine. A program (CUTOFF) facilitates such analyses. It reads in a file that contains the type, charge, and coordinates of each charged atom along with the potential the source produces at that atom. It then offers a menu of ways of selecting specific subsets of atoms. For example, atoms in a given sequence range may be selected; ionized groups and/or polar side chains and/or main chain atoms may be selected; a "center" (usually a source atom) may be specified, and all atoms closer or further than a certain distance from this center may be selected; and residues may be selected by type. The program also makes it possible to step through a range of cutoff radii, calculating the energy for each. The analysis of rhodanese (see "Results") illustrates these various possibilities.

Atom parameters

We report results based on one charge set from the molecular mechanics package AMBER,[34] and on another from parameter set 19 of the package CHARMM.[35] Both treat polar hydrogens explicity but absorb other hydrogens into their parent atoms. The terminal charges were treated by adding a +1 charge to the N-terminal nitrogen and a −1 charge to one C-terminal oxygen.

In the analysis program CUTOFF, we separate the energetic contributions of ionized groups (side chains and backbone termini), nonionized side chains, and main chain atoms. Separating side chain from main chain charges is simple for the CHARMM charge set, because the charges of the main chain atoms (N,C,C_α, O,H) sum to zero. This is not the case for the AMBER charge set, but a reasonable separation may be effected by considering the charge on each C_α to be the superposition of a main chain charge of .246 proton charges and a side chain contribution that depends on the particular side chain. This causes the main chain atom charges to sum to zero and the side chain atom charges to sum to appropriate integer values. The side chain component of the C_α charge is then given by q − .246, q being the total C_α charge. Proline represents a special case in both charge sets, and we treat the entire residue as part of the main chain.

It is necessary to ascertain the locations of polar hydrogens, since these are not included in the crystallographic coordinate sets. The locations of main chain hydrogens are fully determined by the X-ray coordinates, but the locations of some other polar hydrogens are not determined. In the present work, we fix these ambiguous polar hydrogens using the arbitrary assumption of a 180° (trans) dihedral angle, where applicable. (In tyrosine, the dihedral angle is defined relative to Cϵ1.) The three hydrogens of lysine's ammonium are combined into a single charge located at the average coordinates of the three. The lone pair charges on sulfurs are similarly combined and placed at an average location. An additional ambiguity results from the fact that the crystal structure of rhodanese does not distinguish between the amide oxygen and nitrogen in glutamine and asparagine side chains. The present calculations arbitrarily assign the first ambigous atom in each amide as the oxygen.

The low dielectric protein interior is defined as the region contained by the Richards type surface,[36] which is composed of contact and reentrant surface. The shape of the protein was determined using standard united atoms van der Waals radii.[37] Except as otherwise noted, we used a probe whose radius is roughly that of a water molecule (1.4 Å). In certain calculations, we incorporate a Stern layer, a region surrounding the protein where the dielectric constant is that of the solvent, but the ionic strength is zero.[39] This accounts for the fact that the electrolyte's mobile ions cannot overlap the atoms of the protein. In order to incorporate a Stern layer, the part of the finite-difference grid assigned the protein's internal dielectric constant (the dielectric map[18,19]) must be different from the part of the grid assigned zero ionic strength (the ion-exclusion map[18,19]). For a Stern layer of thickness r_S, the protein's atomic van der Waals radii were incremented by r_S, and the probe radius was set to r_S. The process of generating both the dielectric and ion-exclusion maps begins with construction of Lee and Richards surfaces,[38] having point densities of 200 points/atom.

Protein structures

The Brookhaven Protein Data Bank[40] provided the structures of rhodanese (1RHD),[41] BPTI (4PTI),[42] and subtilisin BPN′ (1SBT).[43]

Application of Tanford-Kirkwood Model to Proteins

In the Tanford-Kirkwood model, the four geometric parameters that determine the interaction of any two charges are the radius of the spherical molecule, the distance between the two charges, and the depth of each charge from the sphere's surface. Of these, the results are least sensitive to the sphere radius, and any reasonable choice is adequate. The distance between charges is obtained directly from the crystal structure of the molecule under study. The charge depths, however, while important, are harder to define. In many applications, all charges have been placed at a fixed depth of between 0 and 1 Å below the surface.[3,13,16] This approach is physically plausible for ionizable groups, which are generally exposed to solvent, but is inappropriate for buried atoms. Another approach has been to make the depth of an

ionizable group depend on its relative surface accessibility.[12] However, this will not distinguish between two groups that are both buried, one deeply, and the other nearer the surface.

In the present paper, where many calculations involve deeply buried atoms, we take the depth of a charge below the surface to be the distance to the closest "dot" of the solvent accessible surface, generated using the program MS.[44] With this definition, all charges are at least one van der Waals radius from the surface.

In a few calculations involving subtilisin BPN′, we place the charges very close to the surface. The purpose is to compare with the modified Tanford-Kirkwood model[3], in which all charges are placed 0 Å below the surface, and a surface accessibility correction is applied as well. We are not able to obtain convergence of the Tanford-Kirkwood series solution for a charge at zero depth, so the smallest depth we use is .1 Å. We find that using a depth of 0 yields erratic results. A Stern layer (i.e. an ion-exclusion radius[15]) is incorporated by modifying expression A2 of Gilson et al.[10] to use an ion-exclusion radius different from the dielectric sphere radius.

RESULTS

Calculated pK Shift for His 24 of Subtilisin BPN′

Fersht and coworkers[29,30] have used site-directed mutagenesis to replace either Asp 99 or Glu 156 of the bacterial serine protease subtilisin BPN′ with a serine. Comparison of the wild-type and mutant enzymes' kinetics yields experimental values for the effect of these two charged groups on the pK of His 64, based on the fact that this residue must be neutral for catalysis to occur. Such pK shift data have been obtained for His 64 at a number of ionic strengths. Since Asp 99 and Glu 156 are surface residues more than 10 Å away from His 64, it seems reasonable to assume that the pK shifts they cause result directly from their electrostatic interactions with the ionized form of His 64, using the standard formula $\Delta pK = \Delta G^0/1.4$, with ΔG^0 in kcal/mol. The large distance from His 64 also implies that the dipolar serines substituted for the negatively charged carboxylates produce very small potentials at the histidine.

We have attempted to reproduce the experimental data through calculations of the electrostatic interaction of the charged form of His 64 with the two carboxylates. As already reported, we find reasonable agreement between the calculated and experimental results.[28] In this paper, we explore the effects on the calculated potentials of varying the protein's interior dielectric constant, the thickness of the Stern layer, the dielectric properties of the solvent, and the conformation of the Asp 99 side chain. (Note that in the following discussion, a "large" shift actually means large and negative, since all the pK shifts are less than zero.)

The calculations were performed by placing a unit charge on atom Nϵ2 of the histidine and determining the average potential at the two carboxylate oxygens of Asp 99 and of Glu 156. The results obtained by this procedure are what would be obtained by charging either Asp 99 or Glu 156 individually and calculating the potential at His 64. It is worth pointing out that calculations with either Asp 99 or Glu 156 charged yield an essentially uniform (within ~10%) potential over the ring atoms of His 64, implying that the precise location of the added charge on the ionized histidine is not important to the final result. Also, the calculated potentials at the Asp 99 oxygens were always within ~20% of each other, although the differences were sometimes larger for Glu 156. The potentials at Cγ of Asp 99 were generally ~15% larger than the average potentials at the oxygens, and the potentials at Cβ of Glu 156 were generally ~15% lower than the average potentials at its oxygens. These results imply that delocalization of charge over the side chains should have only moderate effects on the predicted outcome.

As stated in "Materials and Methods," the Lee and Richards dot surfaces used in generating these results started with 200 points per atom. Increasing the number of points to 300 in several test runs produced negligible changes in the calculated potentials (~2%). This implies that the accuracy of the calculations was not limited by the detail used in representing the protein's shape.

In calculating the interaction of subtilisin's Asp 99 with His 64, Asp 99 had to be "built in" approximately, because the Protein Data Bank structure (1SBT) lists an alanine instead of the correct aspartate. The protein modeling program PAKGGRAF[45] was used to determine the most likely location for the side chain, with all other atoms held fixed at their crystallographic locations. This left two degrees of freedom, the χ_1 and χ_2 side chain dihedral angles. The energetically favored conformation (conformation 1) has the following coordinates: Cγ: (7.246, 21.367, 25.565); Oδ1: (6.863, 20.784, 24.571); Oδ2: (6.665, 22.638, 25.878). The distance between Cγ of Asp 99 and Cγ of His 64 for this conformation is 12.9 Å, in agreement with the 13 Å value for the model of Fersht and coworkers,[30] and with the crystallographic result they cite. In order to test the sensitivity of the electrostatic calculations to the placement of Asp 99, two other conformations (conformations 2 and 3), with χ_1 increased by +120° and +300°, were also used.

Tables I and II compare experimental and calculated pK shifts caused by the Asp 99 and Glu 156 mutations, respectively. A number of different models are used to compute the shifts. The models are grouped into those based on our detailed Poisson-Boltzmann calculations with various assumptions for the properties of the protein and solvent and those based on simpler models: ϵ = R, Debye-Huckel theory,

TABLE I. Subtilisin Electrostatics: Experimental and Calculated His 64 pK Shifts on Removal of Asp 99*

System	Ionic strength (M)				
	0.005	0.010	0.025	0.100	0.500
Experiment	0.38	0.42	0.36	0.26	0.10
Detailed Poisson-Boltzmann calculations					
Model I (ϵ_p = 2, ϵ_s = 80, 2 Å Stern xtal H_2O, Asp 99 conf 1)	0.31	0.29	0.25	0.18	0.10
Model Ia (I, but Asp conf 2)	0.30			0.17	
Model Ib (I, but Asp conf 3)	0.30			0.17	
Model II (I, but 0 Å Stern layer)	0.30			0.12	
Model III (I, but 3 Å Stern layer)	0.32			0.21	
Model IV (I, but no xtal H_2O)	0.30			0.16	
Model V (I, but bound H_2O layer)	0.96			0.85	
Model VI (I, but ϵ_p = 1)	0.32			0.19	
Model VII (I, but ϵ_p = 10)	0.26			0.15	
Model VIII (I, but ϵ_p = 78)	0.17			0.10	
Simple models					
Model IX (ϵ = R)	1.2	1.2	1.2	1.2	1.2
Model X (Debye-Huckel theory, with a = 3.5 Å)	0.14	0.11	0.074	0.026	0.0021
Model XI (Tanford-Kirkwood, real depths, ϵ_p = 2)	0.45	0.41	0.38	0.33	0.28
Model XIa (Tanford-Kirkwood, real depths, ϵ_p = 4)	0.34	0.30	0.27	0.22	0.17
Model XII (Tanford-Kirkwood, depths = 1.0 Å)	0.32	0.27	0.24	0.19	0.14
Model XIII (Tanford-Kirkwood, depths = .5 Å)	0.26	0.21	0.17	0.12	0.067
Model XIV (Tanford-Kirkwood, depths = .1 Å)	0.24	0.19	0.15	0.093	0.039

*Experimental and calculated pK shifts of His 64 caused by removal of Asp 99 (negative signs before pK shifts removed to simplify Table). See Note Added in Proof.

and Tanford-Kirkwood theory (see Note Added in Proof). The calculated results at all ionic strengths are presented for the first Poisson-Boltzmann model, in order to show the overall agreement between experiment and theory. These results have already been presented.[28] Results for the other Poisson-Boltzmann models are given at low and high ionic strength only. No results are shown for Glu 156 at 0.500 M because experimental data are not available for this case. Also, the 1.0 M case for both Asp 99 and Glu 156, as well as the 0.005 M result for Glu 156 have been omitted, since the experimental data are uncertain.[46] The result for Glu 156 at 0.001 M was kindly provided by Dr. Alan Fersht.

Comparison with experiment

As previously noted,[28] the experimental results appear to have an error of about ±0.06 pK units, based on the change in pK shift using two different substrates at 0.1 M ionic strength. The two substrates yield shifts of −0.29 ±.03 and −0.23 ±.03, which combine to give a value of −.26 ±.06.

A model that uses physically reasonable parameters yields satisfactory agreement with the experi-

TABLE II. Subtilisin Electrostatics: Experimental and Calculated His 64 pK Shifts on Removal of Glu 156*

	Ionic strength (M)			
System	0.001	0.010	0.025	0.100
Experiment	0.39	0.42	0.41	0.25
Detailed Poisson-Boltzmann calculations				
Model I (2, 80, 2 Å Stern, xtal H_2O, asp conf 1)	0.42	0.37	0.34	0.27
Model II (I, but 0 Å Stern layer)	0.42			0.17
Model III (I, but 3 Å Stern layer)	0.42			0.29
Model IV (I, but no xtal H_2O)	0.57			0.38
Model V (I, but bound H_2O layer)	2.7			2.6
Model VI (I, but $\epsilon_p = 1$)	0.43			0.28
Model VII (I, but $\epsilon_p = 10$)	0.37			0.24
Model VIII (I, but $\epsilon_p = 78$)	0.22			0.14
Simple models				
Model IX (ϵ = R)	1.53	1.53	1.53	1.53
Model X (Debye-Huckel theory, with a = 3.5 Å	0.16	0.13	0.093	0.034
Model XI (Tanford-Kirkwood, real depths, $\epsilon_p = 2$)	0.67	0.62	0.59	0.53
Model XIa (Tanford-Kirkwood, real depth, $\epsilon_p = 4$)	0.47	0.42	0.39	0.33
Model XII (Tanford-Kirkwood, depths = 1.0 Å, $\epsilon_p = 2$)	0.39	0.34	0.31	0.25
Model XIII (Tanford-Kirkwood, depths = .5 Å, $\epsilon_p = 2$)	0.31	0.26	0.22	0.16
Model XIV (Tanford-Kirkwood, depths = .1 Å, $\epsilon_p = 2$)	0.28	0.23	0.19	0.12

*Experimental and calculated pK shifts of His 64 caused by removal of Glu 156 (negative signs before pK shifts removed to simplify Table). See Note Added in Proof.

mental results. Model I uses standard van der Waals radii for the dielectric map, a 2 Å Stern layer (r_S = 2), an interior dielectric constant of 2 ($\epsilon_p = 2$), and a solvent dielectric constant of 78 ($\epsilon_s = 78$), and includes all 17 crystallographic waters as part of the low dielectric protein interior. The agreement with experiment for Glu 156 is quite good, with an rms error between experimental and theoretical pK shifts of 13%, which is comparable with the experimental error. The Asp 99 calculations yield pK shifts that are generally somewhat smaller than the experimental values, especially at low ionic strength. The rms error for Asp 99 over all five ionic strengths is 36%. (Adusting the experimental values toward the theoretical ones by up to .06 pK units yields an rms error of 15% for Asp 99.) Since Asp 99 was "built in" computationally (see above), we explored the consequences of varying the side chain's conformation. The calculated results are insensitive to the conformation of this side chain, as seen in Models Ia and Ib, where χ_1 was changed by 120° and 300°, respectively.

Effects of altering the Stern layer

Reducing the thickness of the Stern layer from 2 Å to 0 Å (Model II) causes the calculated pK shifts to fall, since it allows counterions to come closer to the charged groups. The changes are larger at the higher ionic strength (0.1 M), at which shift changes of 0.06

to 0.10 are observed. As a consequence, the agreement with experiment is not as good.

Increasing the thickness of the Stern layer to 3 Å, Model III, again has little effect on the low ionic strength results and produces a modest increase in the calculated shifts at higher ionic strengths. This improves the agreement with experiment of the calculated results for Asp 99, without markedly perturbing the Glu 156 results. The 3 Å Stern layer thus yields somewhat improved overall results. It is not clear what Stern layer thickness best represents the physical system, since the predominant electrolyte used in the experiments was a sodium/potassium phosphate buffer, containing species with ionic radii ranging from ~1 Å to ~3.5 Å.

Bound surface water effects

Some sites at protein surfaces immobilize waters well enough to produce solvent electron density peaks in X-ray crystallographic studies. The crystal structure for subtilisin BPN′ contains 17 such crystallographic waters, some of them in the active site cleft. In the calculations so far presented, these waters have been included as part of the low dielectric protein interior. This corresponds to an assumption that they are not free to reorient in response to a changing electrostatic field. In Model IV, we examine the effect of treating these waters as bulk solvent. As shown in Table II, this change produces marked increases in the pK shifts for Glu 156 at both low and high ionic strengths. It is initially surprising that increasing the amount of high-dielectric material should strengthen an electrostatic interaction. However, it has been pointed out that introducing a low-dielectric region between two charges in an otherwise high-dielectric environment can weaken their interaction,[47,48] and there is in fact at least one crystallographic water between Glu 156 and His 64. The increased pK shifts for Glu 156 upon treating crystallographic waters as bulk water weaken the agreement with experiment. The agreement with experiment is weakened for Asp 99 also, although here treating the crystallographic waters as bulk water diminishes the interactions with His 64.

While it is clear that crystallographic waters are partially immobilized, it may be that the entire surface of a protein is covered with a layer of waters that, although they are not detected crystallographically, possess a reduced dielectric constant. This idea may be explored by calculating the effect of placing a low-dielectric shell around subtilisin and comparing the theoretical results with experiment. We calculated the effect of assuming an ion-excluding, bound water layer around the protein, with a thickness equal to the diameter of a water molecule (2.8 Å) and a dielectric constant of 2 (the same as the protein interior). This represents a limiting case, in which no dipolar relaxation is considered to occur in response to neutralization of a charged residue. The dielectric map was generated using atomic van der Waals radii incremented by 2.8 Å and a probe radius of 1.4 Å. A zero thickness Stern layer was assumed; therefore ions could approach to the dielectric boundary. This model (Model V), otherwise identical with Model I, yields poor agreement with experiment, with pK shifts of three to ten times the experimental values. The assumption that surface water has a very low dielectric constant thus appears to be inconsistent with the data. It is possible that surface water actually has a dielectric constant intermediate between the values for protein and bulk water. However, since Model I yields good agreement with the data using the bulk water value, it is not necessary to posit altered dielectric properties for water at the protein surface.

Despite the large effect of the 2.8 Å increase in van der Waals radii described here, small changes in van der Waals radii do not produce appreciable effects. Thus, repeating the calculation of Model I with a set of van der Waals radii differing by −.2 to +.25 Å (~.1 Å on average) produced negligible changes in the results.

Effect of changing the protein dielectric constant

In addition to the value $\epsilon_p = 2$, we tested three additional values for the protein dielectric constant: $\epsilon_p = 1$, $\epsilon_p = 10$, and $\epsilon_p = 78$, corresponding to Models VI–VIII. The first and last of these are clearly unrealistic but serve to probe the results of extreme assumptions. The parameters are otherwise identical with those of Model I. Reducing the dielectric constant to 1 has very little effect. Raising it to 10 has a modest effect, shifting the pK by at most 0.05 relative to the result for $\epsilon_p = 2$. Raising it further, to 78, produces a reduction of nearly 50% in pK shifts. That the changes are not greater probably results from the fact that the interactions are heavily screened by the solvent to begin with, so increasing the protein dielectric constant has little additional effect.

Results of simpler models

We examined several models that are simpler than the detailed Poisson-Boltzmann calculations already discussed. The additional results are included in Tables I and II. The simplest model tested is the distance-dependent dielectric constant $\epsilon = R$ (Model IX), which is often used in molecular mechanics simulations. This yields severe overestimates of the pK shifts that are due to both Glu 156 and Asp 99 and does not account for ionic strength effects.

A simple electrostatic model that does include ionic strength effects is Debye-Huckel theory,[49] which is actually a special case solution of the linearized Poisson-Boltzmann equation used in our detailed numerical calculations. Debye-Huckel theory yields the electrostatic potential as a function of the distance from a spherical ion in an electrolyte: $\phi(r) = (q/\epsilon r)\exp(-\kappa r)\{\exp(\kappa a)/(1+\kappa a)\}$, where r is the radial

distance from an ion of radius a and charge q, which is immersed in a solvent having dielectric constant ϵ and ionic strength determined by the Debye-Huckel parameter κ. (The other symbols have their usual meanings.) When applied to subtilisin, this model neglects the facts that the protein does not contain any electrolyte and that it has a low dielectric constant. As a consequence, Model X, which is Debye-Huckel theory implemented with an ion-exclusion radius (a) of 3.5 Å, yields excessively weak potentials. It is interesting to compare the Debye-Huckel results with the calculations for a protein that does exclude ions but has a hypothetical interior dielectric constant of 78 (Model VIII above), because the difference between the two models must result chiefly from the ion-excluding volume of the protein. The ion-excluding property of the protein strongly affects electrostatic interactions at high ionic strengths, although the effect is modest at low ionic strength.

The Tanford-Kirkwood model includes considerably more detail. Another special case solution of the linearized Poisson-Boltzmann equation, Tanford-Kirkwood theory incorporates the low and high dielectric constants of the protein and solvent, respectively, and also accounts for ionic strength effects. However, it does not account for the complicated shape of a protein, but treats the molecule as a sphere. Several methods of correcting for this simplification have been used (see references in "Materials and Methods"), the best known of which belongs to the Modified Tanford-Kirkwood theory.[3] In this model, all charges are placed on the protein-solvent dielectric boundary (depth = 0). The interactions calculated using the Tanford-Kirkwood equations are then multiplied by a factor between 0.02 and 1, which depends on the solvent exposure of the interacting groups.

We present results for several versions of Tanford-Kirkwood theory. All use a dielectric sphere radius of 30 Å, an ion-exclusion radius of 32 Å, a solvent dielectric constant of 78, and, unless otherwise stated, a protein dielectric constant of 2. We take the distances from His 64 to Asp 99 and Glu 156 to be 14 Å and 12.5 Å, respectively. The most straightforward model (Model XI) places charges at depths equal to those seen in the actual protein (see "Materials and Methods"), in this case 1.60 and 1.75 for the carboxylate oxygens and histidine Nϵ2, respectively. As shown in Tables I and II, this model overestimates the pK shifts, especially at high ionic strengths. It is worth mentioning that raising the protein dielectric constant to 4 (Model XIa) for this model improves the agreement substantially, yielding results that are comparable with the detailed Poisson-Boltzmann calculations. The rms error with respect to experiment is 15% for Glu 156 and 31% for Asp 99. The substantial difference between Models XI and XIa shows that in this system the Tanford-Kirkwood model is far more sensitive to the protein dielectric constant than is the detailed Poisson-Boltzmann Model (compare Model I with Model VII).

It is of interest to explore the effect of different assumptions for charge depth in the Tanford-Kirkwood model, particularly since this parameter has received considerable attention.[3,13,16] Depths of 1.0 Å, 0.5 Å, and 0.1 Å are assumed in Models XII, XIII, and XIV, respectively. Good agreement with experiment is obtained with the 1.0 Å depth, but the smaller depths lead to overscreening. This finding is of particular interest in relation to the modified Tanford-Kirkwood model for protein electrostatics, since this model moves all charges to the surface, as in Model XIV, in calculating electrostatic interactions. This leads to substantial overscreening in the present case. The Modified Tanford-Kirkwood model also applies an extra screening factor, mentioned above, which further weakens the interactions. We estimate the screening factors to be .65 for Glu156/His64 and .40 for Asp99/His64. Applying these would lead to severe overscreening of the subtilisin interactions.

Summary of subtilisin findings

The major results of this study may be summarized as follows. 1) A detailed Poisson-Boltzmann model with physically reasonable parameters yields satisfactory agreement with experiment. 2) The agreement with experiment is best when using a Stern layer whose thickness is roughly equal to an ionic radius. 3) Assuming crystallographic waters to be immobilized improves agreement with experiment. 4) Assuming a layer of low-dielectric solvent at the protein surface weakens the agreement with experiment. 5) The results are rather insensitive to the protein dielectric constant. 6) The results are not sensitive to the conformation of Asp 99's side chain. 7) The distance-dependent dielectric constant (ϵ = R) badly overestimates the pK shifts. 8) Tanford-Kirkwood theory can yield results almost as good as the detailed numerical solutions, but it is quite sensitive to parameters (particularly charge depth and protein dielectric constant). 9) The Modified Tanford-Kirkwood model appears to underestimate the pK shifts substantially.

Active Site Potential in Rhodanese

Rhodanese, a seemingly ubiquitous sulfur-transferase,[41] has a number of features that make it interesting from the standpoint of electrostatics. For one thing, it contains a network of salt-bridges, some of which are buried, at the subunit interface. Also, it appears that two positively charged side chains are important in binding the enzyme's negatively charged substrates. Finally, the key side-chain in catalysis is a cysteine (Cys 247) whose pK is shifted downward to 6.5, and which must be in the ionized thiolate form for catalysis to occur.[32] Hol and coworkers have suggested that α-helices D′ and E′ may help shift the pK of Cys 247, since their positive ends are near its sulfur.[32]

The contributions of various elements of the protein structure to the stabilization of the thiolate ion were

TABLE III. Rhodanese: Interactions With Active Site Thiolate*

Model	Total	Ionizables	Main-chain	Helix D′	Helix E′	Gly 250
Detailed Poisson-Boltmann models						
Ia (ϵ_{prot} = 2, r_S = 2 Å, CHARMM)	−22.10	−0.51	−24.99	−10.18	−5.35	−7.18
Ib (ϵ_{prot} = 2, r_S = 2 Å, AMBER)	−16.21	−1.98	−18.47	−5.63	−4.05	−6.51
II (ϵ_{prot} = 5, r_S = 2 Å, CHARMM)	−11.83	−1.09	−12.12	−4.89	−2.43	−3.04
III (ϵ_{prot} = 2, r_S = 0 Å, CHARMM)	−19.81	0.49	−23.97	−9.29	−5.25	−7.27
Simpler models						
IV (T-K,† ϵ_p = 2, CHARMM)	−13.18	0.07	−18.59	−7.28	−3.42	−6.17
V (ϵ = R, CHARMM)	−43.48	−4.21	−39.93	−14.23	−4.12	−11.14
VI (ϵ = 2, CHARMM)	−103.95	−50.37	−57.00	−20.40	−9.19	−9.32

*Interaction energy of components of rhodanese with active site thiolate. Total: all charges; ionizables: only chain termini and charges of ionizable side chains; main chain: charges of all main chain atoms; helix D′: charges of main chain atoms of residues 251–264; helix E′: main chain atoms of residues 274–282; Gly 250: main chain atoms of Gly 250. (Interactions with atoms of Cys 247 excluded in all cases.)
†Tanford-Kirkwood.

calculated by performing a detailed Poisson-Boltzmann calculation with only Cys 247's sulfur charged (−1), and determing the potential at each other charged atom in the protein (see "Materials and Methods"). In these calculations, the dielectric map omitted the persulfide S included on Cys 247 in the Protein Data Bank structure, as this could not have been present in the titration experiments. The results presented here exclude contributions from the atoms of Cys 247 itself. All lysines, aspartic acids, glutamic acids, arginines, and histidines were assumed fully charged, as were both chain termini. Models Ia and Ib (see Table III) assume a protein dielectric constant of 2, a 2 Å Stern layer, a solvent dielectric constant of 80, and physiological ionic strength. They differ only in the choice of charge set, employing CHARMM and AMBER, respectively. We also tested the effects of varying the protein dielectric constant and the Stern layer thickness by using two additional parameter sets. Models II and III are the same as Model Ia, except that they use, respectively, a protein dielectric constant of 5 and a zero thickness Stern layer.

Contributions to stabilization of Cys 247 thiolate

The contributions of various parts of rhodanese to the potential at the sulfur of Cys 247 are detailed in Table III. Here we focus on the results of Model Ia. The consequences of altering parameters are reported below. Because of the arbitrary locations of many ambiguous polar hydrogens and the uncertain orientation of amide side chains (see "Materials and Methods"), the electrostatic interactions of polar side chains have not been carefully examined. Since the reported total interaction energies (Table III) include the contributions of polar side chains, they should be viewed as uncertain, even within the context of the present model.

The total electrostatic stabilization of the thiolate is found to be −22 kcal/mol (Table III). Taken by itself, this would shift the Cys 247 pK down by 16 pK units. The observed downward shift is only about 2.5 units. The large discrepancy between these values might become larger if polar hydrogens were placed more carefully, because several serines and threonines (notably Ser 274[32]) probably form hydrogen bonds or short-range charge-dipole interactions with the thiolate. On the other hand, the discrepancy is expected to decrease upon accounting for the solvation energy of the partially buried thiolate (see "Discussion").

The small effect of ionized groups on the potential at the thiolate is notable. Closer examination shows that this small net effect represents a balance between the stabilizing effect (−6 kcal/mol) of the eight histidines (here assumed fully charged) and the destabilizing effect of other ionized groups. The peptide chain's terminal charges produce negligible effects.

Most striking perhaps is the large stabilization (−25 kcal/mol) provided by main chain atoms. This is almost entirely accounted for by a local (hydrogen bonding[32]) interaction with the amide nitrogen of Gly 250 (−7 kcal/mol), and longer range interactions with α-helices D′ and E′ (−16 kcal/mol). (The main chain atoms of Cys 247 contribute about −3 kcal/mol to the thiolate's stability. However, a similar contribution is likely to be present for a cysteine in solution, so

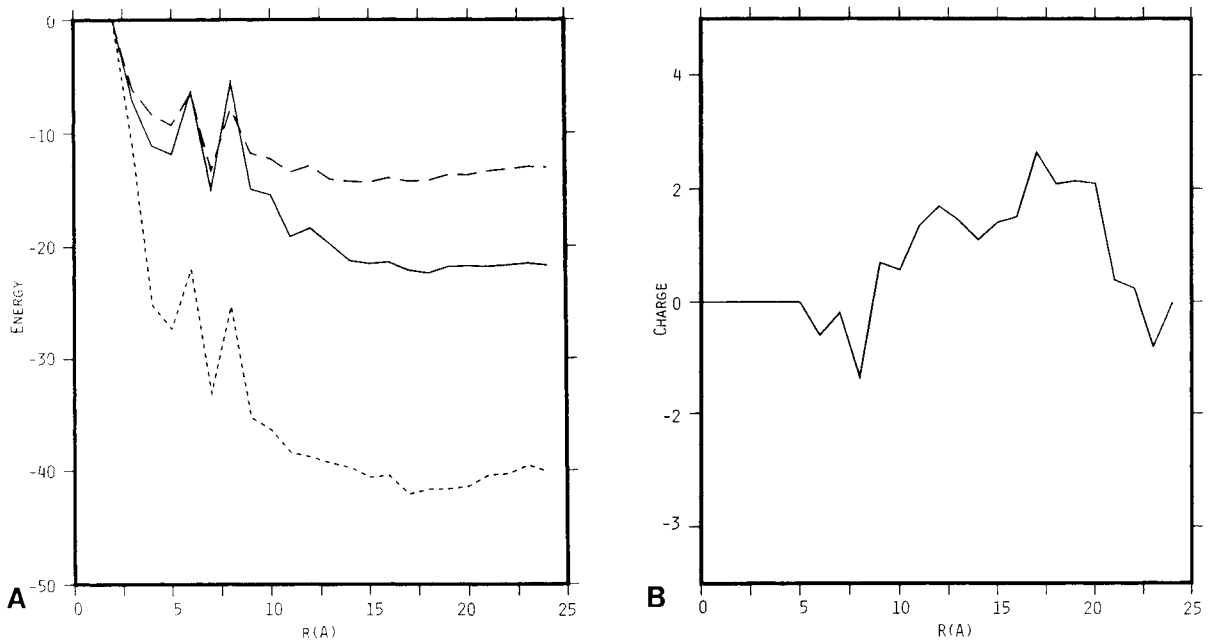

Fig. 1. **A:** Electrostatic interaction energy (kcal/mol) of Cys 247 thiolate with all other charged atoms (real and partial) of rhodanese (excluding Cys 247) as a function of radius (Å) of a cutoff sphere centered on the thiolate. Solid curve: detailed Poisson-Boltzmann. Dashed curve: Tanford-Kirkwood. Dotted curve: ϵ = R. **B:** Total charge enclosed by cutoff spheres.

this contribution probably has little effect on the group's pK in rhodanese.)

Range of electrostatic interactions

In this section, we examine the range of interactions influencing the pK of the active site Cys 247 in rhodanese. The calculations avoid splitting neutral groups by including either all or none of each residue's main chain atoms and all or none of each non-ionized residue's side chain, depending on whether the residue's main chain nitrogen falls within the cutoff radius. However, the atoms of ionized side chains are included solely on the basis of whether they fall within the cutoff sphere. The stabilization of the thiolate by all atoms, charged and partially charged, as a function of the radius of a cutoff sphere centered on the sulfur atom is presented in Figure 1A (solid line). For comparison, Figure 1B plots total charge as a function of cutoff radius.

The change in electrostatic stabilization becomes small at a distance of about 15 Å from the sulfur. Ionized groups produce a negligible overall effect (when the histidines are considered charged—see above), but their contributions fluctuate greatly between 5 and 11 Å from the sulfur, attaining a maximal (destabilizing) effect of +11.2 kcal/mol at a cutoff radius of 8 Å (see Fig. 2). Thus, ionizable groups can make large contributions to electrostatic potentials at a range of at least 10 Å, although in rhodanese their effects are mutually cancelling. This point is illustrated in Figure 3, which shows the contributions of the eight histidines alone, as a function of cutoff radius. The histidine side chain atoms beyond 10 Å from the thiolate contribute about −4 kcal/mol. The long effective range of neutral dipolar groups is also quite striking, as seen in Figure 4. Although they contribute only −1.6 kcal/mol beyond 10 Å, the ~3 kcal/mol fluctuation in their contribution between 10 and 15 Å suggests that they are capable of producing larger long-range effects.

The long-range contributions of neutral dipolar groups are due primarily to the main chain atoms of helices D′ and E′, whose influence as a function of cutoff radius is shown in Figure 5A (solid line). The curve shows a monotonic decline up to ~16 Å. Almost 40% (−6 kcal/mol) of the energy is due to residues further than 7 Å from the thiolate, and almost 20% (−3 kcal/mol) is due to residues beyond 10 Å. In contrast, the other main chain atoms (Fig. 5A, dashed line) contribute irregularly with distance, and much of the stabilization is short range. Figure 5B shows the number of atoms (N, C, O, Cα, H) belonging to helices D′ and E′ (solid curve) and to all other main chain atoms (dashed) and highlights the fact that the two helices provide greater stabilization than the other main chain atoms yet include a far smaller number of residues.

Sensitivity to charge set

We found substantial differences between results based on the AMBER and CHARMM charge sets.

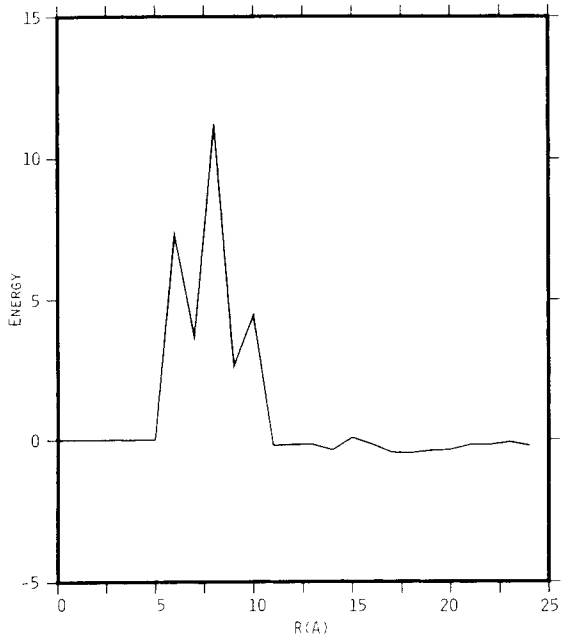

Fig. 2. Electrostatic interaction energy (kcal/mol) of Cys 247 thiolate with all ionized groups (side chains and main chain termini), as a function of radius (Å) of a cutoff sphere centered on the thiolate. Calculated using detailed Poisson-Boltzmann model.

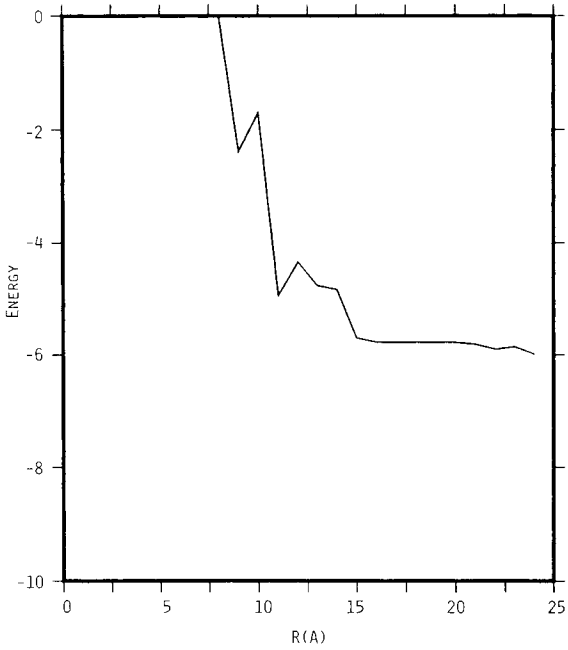

Fig. 3. Electrostatic interaction energy (kcal/mol) of Cys 247 thiolate with all histidine side chains, assumed ionized, as a function of radius (Å) of a cutoff sphere centered on the thiolate. Calculated using detailed Poisson-Boltzmann model.

Model Ib (Table III) uses the same parameters as Model Ia, except that it uses the AMBER charge set. The overall stabilization of the thiolate decreases by 6 kcal/mol, and the contributions of various elements of the protein do not change in a consistent manner. For example, the stabilization by ionized groups increases by 1.5 kcal/mol, while the stabilization by main chain atoms falls by 6.6 kcal/mol.

The change in helix stabilization is particularly interesting. When AMBER is used, the contribution from helix D′ is 0.56 of its value based on the CHARMM charge set, and the contribution from helix E′ is down by a factor of 0.76. One cause of this difference is the fact that the dipole moment of the main chain atoms in the CHARMM charge set is 4.3 Debye, while that in AMBER is 3.8 Debye, down by a factor of 0.88. However, this is not sufficient to explain the observed energy decrements. Most of the remaining effect appears to result from the fact that the peptide dipole moments in the two charge sets are oriented differently by ~14°. The mean angle with respect to an α-helix axis is ~37° for the CHARMM charge set and ~49° for the AMBER set. This leads to a further reduction in helix dipole moment by .82 (=cos49°/cos37°) for AMBER relative to CHARMM. Combined with the reduced magnitude AMBER's peptide dipole moment, the net reduction in helix dipole moment is a factor of 0.72. This corresponds well with the reduction in interaction of helix E′. The greater effect for helix D′ is apparently connected with the fact that this helix does not point directly toward the thiolate sulfur.

Sensitivity to ϵ_p and Stern layer thickness

Since the dielectric constant of a protein remains somewhat undertain, it is important to test the degree to which varying this parameter affects the result for rhodanese. Repeating our calculations with a protein dielectric constant of 5 (Model II, Table III) weakens most interactions by roughly a factor of 2/5. The range of the interactions is reduced, although in percentage terms long-range interactions are as important as before. The general weakening of interactions upon increasing the protein's dielectric constant is not surprising, since their initial strength implies that the solvent screening is weak, causing the results to depend largely on the protein dielectric constant.

Our results are nearly independent of the choice of Stern layer, as illustrated by the results for Model III (Table III), where the Stern layer is of zero thickness. The total interaction energy is reduced by a factor of about 0.9, the interaction with helices D′ and E′ is reduced by about 0.93, and the range of interactions is essentially unchanged. The change in sign of the interaction with ionized groups results from the fact that this value is a balance between larger stabilizing and destabilizing effects. The stabilizing groups apparently are more subject to solvent screening, so decreasing the Stern layer masks their effects and produces a destabilization. Conversely, increasing the protein's dielectric constant masks the effects of the destabilizing groups and leads to a net stabilizing result for the ionized groups.

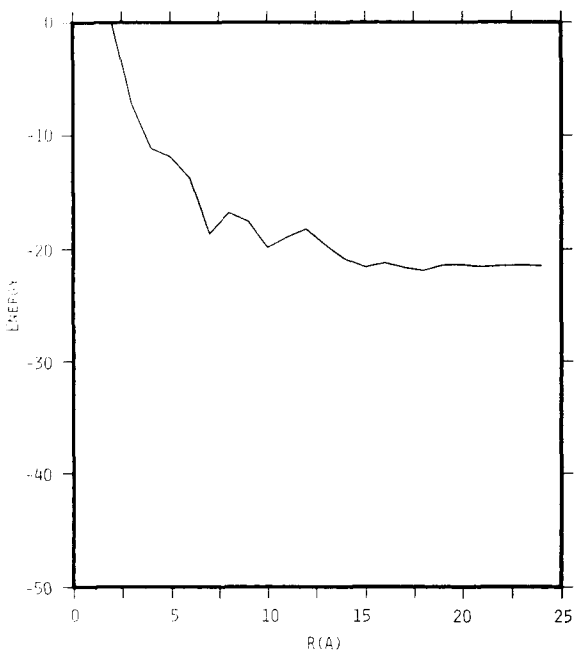

Fig. 4. Electrostatic interaction energy (kcal/mol) of Cys 247 thiolate with all neutral dipolar groups (both main chain atoms and atoms of neutral side chains), as a function of radius (Å) of a cutoff sphere centered on the thiolate. Calculated using detailed Poisson-Boltzmann model.

Comparison with simpler models

The present analysis of electrostatics in rhodanese provides an additional opportunity to compare our detailed Poisson-Boltzmann calculations with the results of simpler models for protein electrostatics. Comparisons are presented in Table III for the Tanford-Kirkwood model (Model IV), the distance-dependent dielectric model (Model V), and a simple Coulomb's law model with $\epsilon = 2$ (Model VI). The Tanford-Kirkwood model here uses actual charge depths (see "Materials and Methods"), a probe radius of 1.4 Å, a Stern layer of 2 Å, a dielectric sphere radius of 30 Å, and other parameters in accordance with the detailed Poisson-Boltzmann calculation of Model Ia. These three simpler models all use the CHARMM charge set.

The Tanford-Kirkwood model yields a total stabilization that differs from the detailed Poisson-Boltzmann result by a factor of 0.6. The various components of this total listed in Table III show uneven agreement with the detailed calculations but reproduce the general trends well. There is an overall tendency to underestimate the strength of the interactions, which reduces their effective range (Fig. 1A, dashed line). The weakness of the interactions here, relative to those of Model Ia which incorporates the actual shape of the protein, presumably results from the fact that Cys 247 lies in a cleft rather than in a convex part of the protein's surface, so the thiolate is in fact partially removed from solvent. However, because it does form part of the protein surface, the Tanford-Kirkwood model screens it as much as any other surface group.

The distance-dependent ($\epsilon = R$) model provides worse agreement with the detailed calculations of model Ia, and shows a tendency to overestimate the strength of the interactions. For example, the total interaction energy is almost twice that of Model Ia. Such overestimates on the part of this Model have already been noted in this paper. The overestimation is not completely consistent, however. For example, $\epsilon = R$ yields a slightly weaker interaction for helix E′. The range of interactions (Fig. 1A, dotted line) is quite long for this model, with contributions of several kcal/mole occuring as much as 15–20 Å away.

The Coulomb's law model yields a total interaction energy almost five times larger than the detailed Poisson-Boltzmann result. The range of interactions is well over 25 Å (Fig. 6). The complete neglect of solvent effects in this model thus produce severe disagreement with the other models tested.

Summary of rhodanese findings

1) The active site thiolate is stabilized primarily by charge-dipole interactions. 2) Most of the stabilization results from α-helices D′ and E′. 3) Specific short-range charge-dipole interactions are also important. 4) Ionized groups contribute negligibly (when all are assumed fully charged). 5) Both neutral dipolar groups and ionized groups can make significant contributions at ranges of greater than 10 Å, but, in this case at least, the interactions die off by ~15 Å. 6) Tanford-Kirkwood theory agrees fairly well with the detailed Poisson-Boltzmann results. 7) $\epsilon = R$ overestimates the net effect approximately twofold. 8) Coulomb's law with $\epsilon = 2$ overestimates the net effect approximately fivefold. 9) The effect of the α-helices falls ~40% when AMBER charges are used instead of CHARMM charges. 10) The effects are sensitive to the assumed protein dielectric constant.

General Results for Charge–Charge Interactions

Potential versus distance

The preceding sections concern specific cases of charge–charge interactions. Here we consider the general relationship between the distance separating two charges and the screening of their electrostatic interactions. The range of electrostatic interactions in proteins bears on problems of protein design: i.e., to what degree can remote parts of a protein exert significant effects on structural stabilization and on protein function. Moreover, this study relates directly to molecular mechanics simulations, in which screening is often assumed to be a function of charge-charge distance and in which nonbonded cutoffs are commonly used. The present section provides a picture of the relationship between distance and screening in two globular proteins. This relationship is expected to depend on the degree to which charges are removed

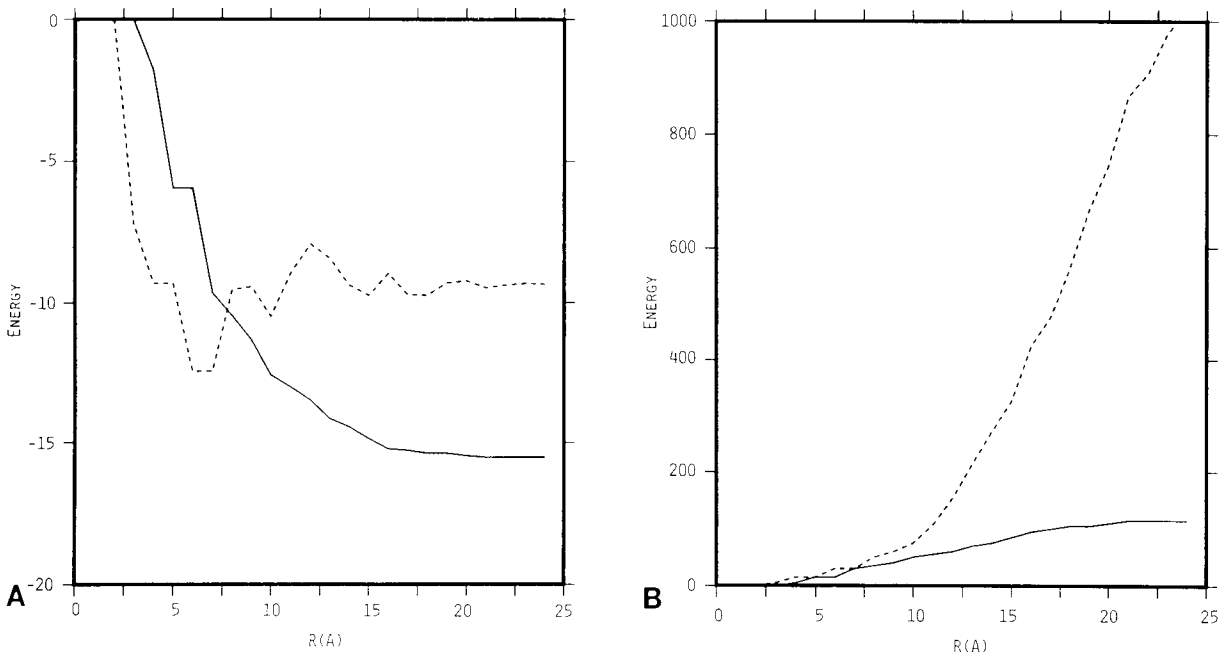

Fig. 5. **A:** Electrostatic interaction energy (kcal/mol) of Cys 247 thiolate with main chain atoms of rhodanese as a function of radius (Å) of a cutoff sphere centered on the thiolate. Calculated using detailed Poisson-Boltzmann model. Solid: helices D' & E' (residues 251–264, 274-282). Dotted: all other main chain atoms. **B:** Numbers of main chain atoms corresponding to A.

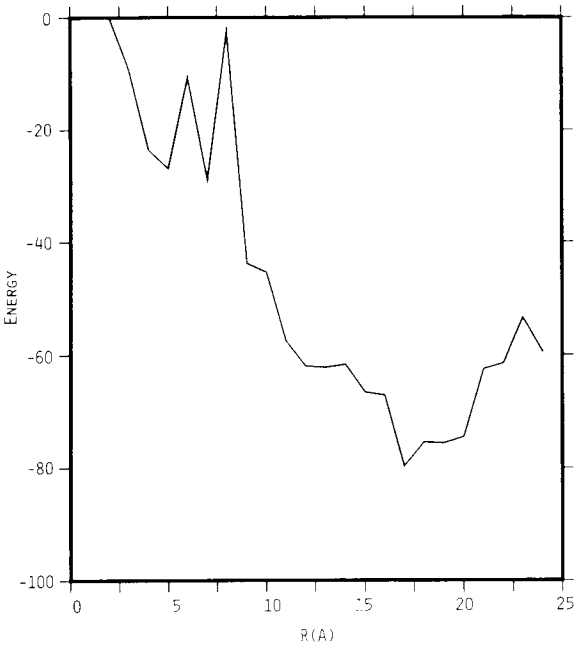

Fig. 6. Electrostatic interaction energy (kcal/mol) of Cys 247 thiolate with all other charged atoms (real and partial) of rhodanese (excluding Cys 247) as a function of radius (Å) of a cutoff sphere centered on the thiolate. Calculated using Coulomb's law with $\epsilon = 2$.

from solvent, as well as on the size of the protein to which they belong. We therefore include results for both surface and buried charges, in rhodanese, a large protein of 293 residues, and in BPTI, a small protein of 56 residues. The calculations also explore the effects of ionic strength on the interactions. The results presented here are subsequently compared with corresponding results generated by the distance-dependent ($\epsilon = R$) model and by the Tanford-Kirkwood model.

For either rhodanese, or BPTI, a single atom (source) was considered to have a unit charge, and the potential at each other charge-bearing atom (target) was calculated, using a protein dielectric constant of 2, a solvent dielectric constant of 80, a 2 Å Stern layer, and either physiological (Debye length of 8 Å) or zero ionic strength. Note that the results of these calculations are potentials, not interaction energies, and are therefore independent of the charges on the target atoms. For each protein, one solvent-exposed atom and one deeply buried atom were used as unit source charges. In order to eliminate internal cavities, which would produce misleading charge depths in the subsequent Tanford-Kirkwood calculations, a 2.5 Å probe was used in generating the dielectric and ion-exclusion maps and in calculating charge depths. (However, a test calculation using a 1.4 Å probe yielded very similar results in this potential-versus-distance analysis.)

Plots of potential versus distance from a surface charge in rhodanese, at physiological and zero ionic

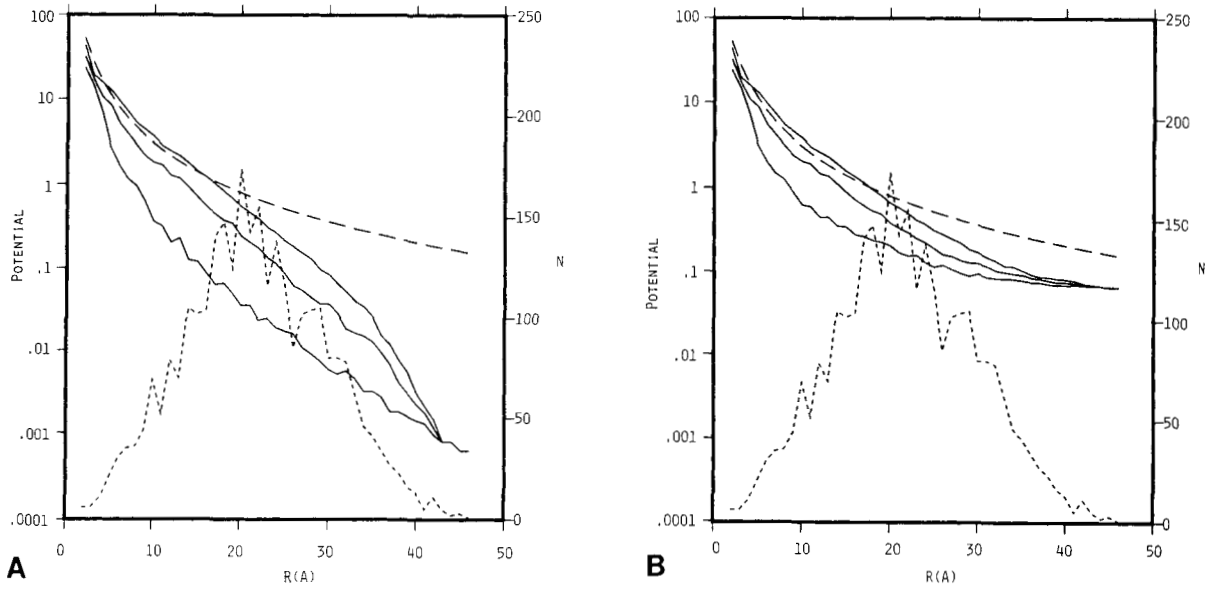

Fig. 7. Electrostatic potentials (kcal/[mol-e$^+$]) caused by a unit charge at rhodanese's surface (left ordinate), and number of charge-bearing atoms (right ordinate) as a function of distance (Å) from the source charge. Distances are divided into 1 Å bins. Solid curves: maximum, minimum, and average potentials found within each distance bin. Dotted curves: number of charge-bearing atoms in each bin. Dashed curves: results for ϵ = R. **A:** Physiological ionic strength (0.15 M). **B:** Zero ionic strength.

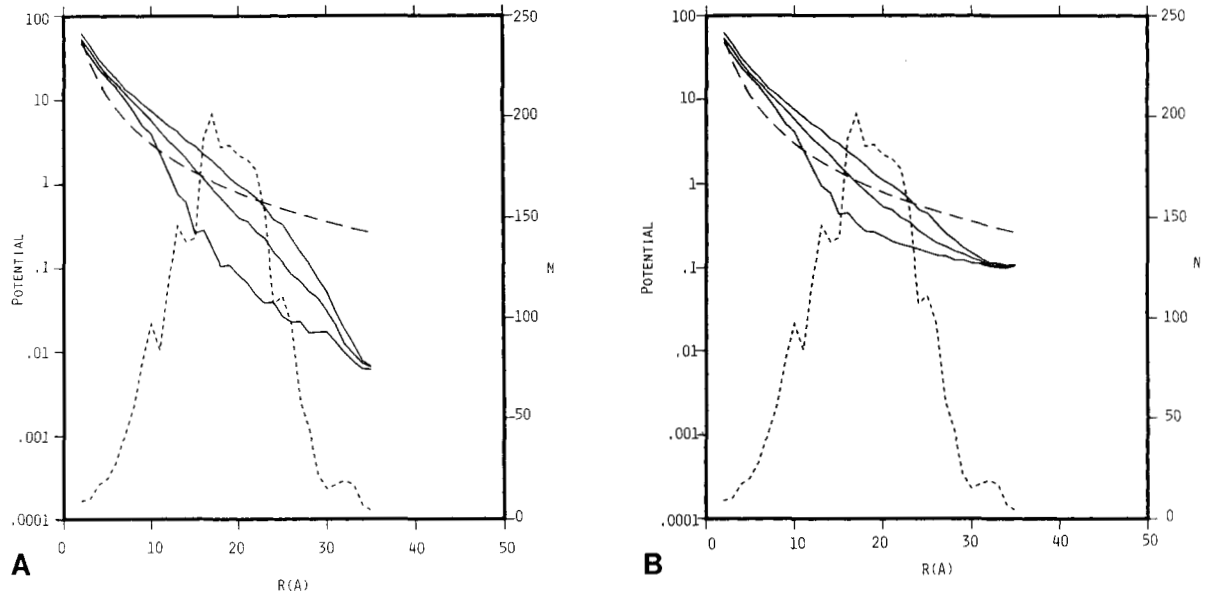

Fig. 8. Electrostatic potentials (kcal/[mol-e$^+$]) caused by a buried unit charge in rhodanese (left ordinate), and number of charge-bearing atoms (right ordinate), as a function of distance (Å) from the source charge. Distances are divided into 1 Å bins. Solid curves: maximum, minimum, and average potentials found within each distance bin. Dotted curves: number of charge-bearing atoms in each bin. Dashed curves: results for ϵ = R. **A:** Physiological ionic strength (0.15 M). **B:** Zero ionic strength.

strength, are shown in Figure 7A and B, respectively. The source charge is the main chain N of Ala 8, which is 1.65 Å deep. As expected, potentials fall with distance from the source. The scatter is quite large, however (note the logarithmic ordinate). At a distance of 20 Å, roughly the most probable charge–charge distance in this case, potentials vary by about a factor of 10 (.03–.5 kcal/[mol-e$^+$]) at physiological ionic strength, and by about a factor of 3 (.2–.7 kcal/[mol-e$^+$]) at zero ionic strength. Electrostatic potentials as large as 1 kT/e (0.6 kcal/[mol-e$^+$]) are found up to ~20 Å away at both physiological and zero

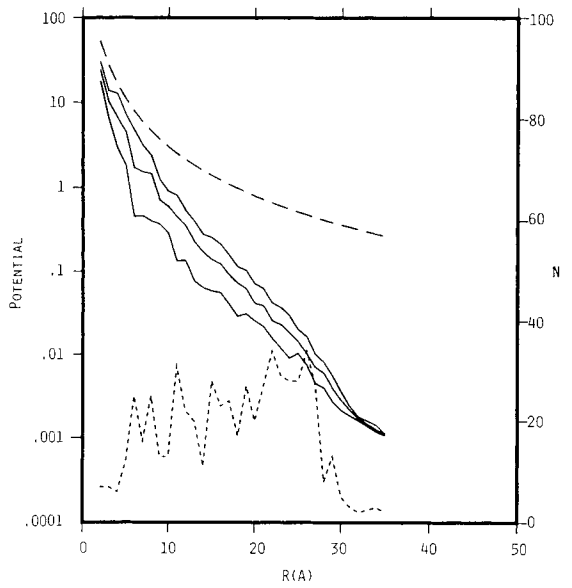

Fig. 9. Electrostatic potentials (kcal/[mol-e$^+$]) caused by a unit charge at BPTI's surface (left ordinate), and number of charge-bearing atoms (right ordinate) as a function of distance (Å) from the source charge. Distances are divided into 1 Å bins. Solid curves: maximum, minimum, and average potentials found within each distance bin. Dotted curve: number of charge-bearing atoms in each bin. Dashed curve: results for ϵ = R. Physiological ionic strength (0.15 M).

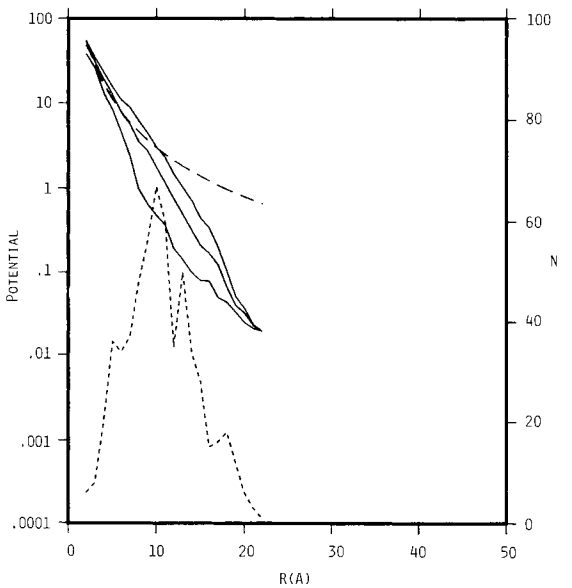

Fig. 10. Electrostatic potentials (kcal/[mol-e$^+$]) caused by a buried unit charge in BPTI (left ordinate), and number of charge-bearing atoms (right ordinate), as a function of distance (Å) from the source charge. Distances are divided into 1 Å bins. Solid curves: maximum, minimum, and average potentials found within each distance bin. Dotted curve: number of charge-bearing atoms in each bin. Dashed curve: results for ϵ = R. Physiological ionic strength (0.15 M).

ionic strength. The physiological and zero ionic strength results are similar at close range (up to about ~8 Å). At longer distances, the increased screening of the ions becomes important. For physiological ionic strength, effective dielectric constants of up to 10,000 are seen, but the maximum value for zero ionic strength is about 120. The occurrence of effective dielectric constants larger than the dielectric constant of the solvent has been discussed previously.[10,48]

Similar calculations using a deeply buried source charge in rhodanese are shown in Figure 8A,B. Here the source is the main chain N of Val 111, which is 11.1 Å below the surface. The potentials are significantly larger than those generated by the surface atom, and the amount of scatter slightly less. Potentials of kT/e$^+$ here occur out to ~23 Å for both physiological and zero ionic strength. The maximum effective dielectric constants seen for physiological ionic strength are about 1,500 and 100 for physiological and zero ionic strength, respectively.

These general results are not expected to be particular to the atoms chosen a sources, and in fact, very similar results are found using a different surface atom (N of Glu 218) and a different buried atom (N of Cys 254) at both ionic strengths (results not shown).

Corresponding results for the small protein BPTI are shown in Figures 9 and 10, for physiological ionic strength only. These results permit comparison between the electrostatic interactions in a large and a small protein. The surface charge used here (Fig. 9) is the main-chain N of Ala 16 (1.65 Å deep), and the buried charge (Fig. 10) is the main chain of N of Phe 22 (5.9 Å deep). The forms of the BPTI curves are similar to those of rhodanese however the scatter is less, and the potentials are generally smaller for any distance. The latter is as expected because potentials are more screened in a smaller protein in which the high-dielectric solvent is closer to all atoms. Potentials of kT/e$^+$ are found to distances of about 12 Å and 14 Å for physiological and zero ionic strength, respectively.

An interesting feature of the graphs of potential versus distance is the tendency to display an exponential decline, which is apparent as a roughly linear plot because of the logarithmic ordinate. This tendency is not limited to physiological ionic strength, as shown in Figure 8B, although it is not seen for the surface charge in rhodanese at zero ionic strength (Fig. 7B).

Comparison with simpler models

The previous section shows that that the results of the Poisson-Boltzmann equation cannot be accurately reproduced by any function that depends solely on charge–charge distance, including the distance dependent dielectric functions often used in molecular simulations. Still, a detailed comparison with the results of such a function is of considerable interest, since it is so commonly used. Here we compare the general results just described with corresponding results generated using a distance-dependent dielectric model, ϵ = R. We also compare with the more comprehensive Tanford-Kirkwood model, which accounts for the effect of charge burial on solvent screening.

TABLE IV. Comparisons of $\epsilon = R$ and Tanford-Kirkwood Theory With Poisson-Boltzmann Results*

System	P-B potentials range	N	<PB>	(s.d.)	Distance-dependent rms error (%)	Distance-dependent <Ratio>	Tanford-Kirkwood rms error (%)	Tanford-Kirkwood <Ratio>
Rhodanese,	0–1	2,494	0.20	(.23)	2,700	14	190	1.9
shallow q,	1–10	431	2.5	(1.8)	85	1.5	23	88
I = .15 M	10–100	24	18	(8.8)	56	1.4	8.9	0.93
Rhodanese,	0–1	1,779	0.33	(.27)	730	5	360	3.3
deep q,	1–10	1,033	3.4	(2.3)	36	0.71	24	1.1
I = .15 M	10–100	137	20	(12)	46	0.56	3.7	1.0
Rhodanese,	0–1	2,429	0.30	(.23)	180	2.7	34	1.2
shallow q,	1–10	496	2.5	(1.8)	69	1.4	20	0.91
I = 0 M	10–100	24	19	(8.8)	55	1.4	8.5	0.93
Rhodanese,	0–1	1,692	0.43	(.24)	123	2.0	110	2.0
deep q,	1–10	1,118	3.3	(2.2)	37	0.70	25	1.2
I = 0 M	10–100	139	20	(12)	46	0.55	3.7	1.0
BPTI,	0–1	507	0.14	(.21)	4,300	29	440	4.6
shallow q,	1–10	71	2.8	(1.9)	260	3.3	62	1.5
I = .15 M	10–100	12	19	(6.8)	110	2.1	15	1.1
BPTI,	0–1	248	0.38	(.30)	990	8.2	440	4.4
deep q,	1–10	271	3.5	(2.2)	74	1.5	51	1.4
I = .15 M	10–100	71	19	(11)	15	0.90	8.2	1.1

*Comparision of distance-dependent ($\epsilon = R$) potentials and Tanford-Kirkwood potentials with linearized Poisson-Boltzmann potentials, separated into ranges according to the Poisson-Boltzmann results, for shallow and deep source charges in two proteins. N: number of target atoms falling in given potential range; <PB>: average Poisson-Boltzmann potential over these atoms; s.d.: standard deviation of potentials over these atoms. For each system and each range, rms errors of the distance-dependent and Tanford-Kirkwood models relative to the Poisson-Boltzmann results are given, as are the average ratios of the distance-dependent and Tanford-Kirkwood potentials to the Poisson-Boltzmann potentials.

In implementing the Tanford-Kirkwood model, charge depths are obtained as described in "Materials and Methods", using as 2.5 Å probe sphere in agreement with the dielectric and ion-exclusion maps used in the detailed Poisson-Boltzmann calculations. Dielectric sphere radii of 30 and 20 Å are used for rhodanese and BPTI, respectively. (Varying the radii over several Angstroms has little effect on the results.) Ionic strengths, internal and external dielectric constants, and Stern layers are the same as used in the corresponding detailed Poisson-Boltzmann runs.

Graphic comparisons of the distance-dependent model with the detailed Poisson-Boltzmann results are presented in Figures 7–10. The best agreement is obtained for rhodanese at zero ionic strength (Figs. 7B, 8B). The agreement is not as good for rhodanese at physiological ionic strength (Figs. 7A, 8A), especially for weak interactions at long distances, where the distance-dependent model may overestimate the Poisson-Boltzmann results by more than an order of magnitude. (Note that the logarithmic ordinate causes substantial absolute errors to appear rather small.) Relatively poor agreement is found for the surface charge in the small protein BPTI at physiological ionic strength (Figs. 9, 10), where $\epsilon = R$ severely overestimates most interactions.

Quantitative comparisons of the distance dependent and Tanford-Kirkwood models with the full Poisson-Boltzmann solutions described in the previous section are detailed in Table IV, which presents the rms percentage error between the two simpler models and the Poisson-Boltzmann solutions, as well as average ratios of the results of each model to those of the full solution. These quantities summarize the overall quality of agreement, and indicate whether the simple models tend to over or underestimate the Poisson-Boltzmann results. Because different levels of agreement exist for weak and strong interactions, we provide separate comparisons for potentials between 0 and 1 kcal/(mol-e^+), 1 and 10 kcal/(mol-e^+), and 10 and 100 kcal/(mol-e^+), as determined from the Poisson-Boltzmann calculations. Table IV also gives the number (N) of target atoms for which the potential falls within each potential range, the average potential over these atoms (<PB>), and the standard deviation of the potential over these atoms (s.d.).

Overall, the Tanford-Kirkwood and $\epsilon = R$ models agree surprisingly well with the detailed calculations, as indicated by the rms errors (Table IV). However, the Tanford-Kirkwood model yields substantially lower rms deviations than does the distance-dependent model. For potentials greater than 1 kcal/(mol-e^+), Tanford-Kirkwood theory and $\epsilon = R$ yield rms errors of 4–62% and 15–260%, respectively. A striking result of these comparisons is the tendency of the simpler models to overestimate weak potentials, as indicated by the average ratios shown in Table IV. This is particularly marked for the distance-

dependent model, which on average overestimates them by between 2 and 30 times. Not surprisingly, the greatest disagreement occurs in the presence of a non-zero ionic strength. The Tanford-Kirkwood theory, which includes ionic strength effects, also underestimates weak potentials as high ionic strength, but only by factors of 2 to 5, on average. Because weak potentials are far more numerous than strong potentials (see Table IV), the errors associated with $\epsilon = R$ might have a substantial effect on the course of a molecular simulation.

The agreement of the distance-dependent and Tanford-Kirkwood models with the detailed calculations is much better for the stronger interactions. The Tanford-Kirkwood model produces especially good results. The results for the distance-dependent model depend on the depth of the source charge, with overestimates obtained for the shallow sources and underestimates obtained for the deep sources. It should be pointed out that the deep source charges used here are atypical because they are the deepest main chain nitrogens in each protein.

Summary of general results for charge-charge interactions

1) A unit charge produces potentials of kT/e^+ at distances as large as ~20–25 Å in rhodanese, and ~10–15 Å in BPTI. 2) $\epsilon = R$ overestimates potentials less than 1 kcal/(mol-e^+) by about twofold at zero ionic strength and about an order of magnitude at physiological ionic strength. 3) $\epsilon = R$ agrees much better for potentials greater than 1 kcal/(mol-e^+) but still shows rms errors of 15–260% in this range. 4) Tanford-Kirkwood theory also tends to overestimate weak interactions, but to a smaller degree than $\epsilon = R$. 5) Tanford-Kirkwood theory agrees fairly well with the detailed Poisson-Boltzmann results, especially for potentials greater than 1 kcal/(mol-e^+), for which rms errors of 4–62% are obtained.

DISCUSSION

Calculation of Subtilisin pK Shifts

The pK shifts calculated using the detailed linearized Poisson-Boltzmann solutions are in reasonable agreement with experiment. The agreement is especially good given that the linearized Poisson-Boltzmann equation is inaccurate at the higher ionic strengths used here, at least in the special case of the Debye-Huckel theory for ionic activity coefficients.[49] The calculated pK shifts are remarkably insensitive to moderate changes in the internal dielectric constant of the protein. However, incorporating a nonzero Stern layer is important in reproducing the experimental results at the higher ionic strengths.

Assuming a layer of bound, low-dielectric water at the protein surface leads to marked overestimates of the experimental results. It is not particularly surprising that water molecules at the protein surface would reorient in response to the complete neutralization of charged groups. In addition, even if there is a layer of immobilized water at the protein surface, this immobilization need not lead to a low dielectric constant, as is made clear by the fact the the dielectric constant of ice is as high as that of water. On the other hand, our results suggest that crystallographically localized solvent molecules should be treated as part of the protein rather than as part of the high-dielectric solvent.

One concern regarding the present treatment is that it neglects possible "indirect" effects on the pK of His 64. These would result if a neighboring titratable group's ionization state were altered by the removal of Asp 99 or Glu 156, and if this change altered the potential at His 64. Any such effect would tend to reduce the observed pK shift of His 64. Our calculations yield only the direct effect, and they essentially agree with the experimental results. Thus, if an indirect effect existed, this would imply that the calculations were underestimating the direct effects of Asp 99 and Glu 156 on the pK of His 64. However, Fersht and coworkers report that the measured titration curves of His 64 are characteristic of single ionizations, implying that indirect effects are absent.[29]

One might speculate about the effects of ionic strength on the average conformation of charged side chains in the vicinity of Asp 99 and Glu 156, as conformational changes would influence the potential at His 64. It is also possible that replacing Asp 99 by a serine leads to conformational changes in other charged groups sufficient to perturb the pK of His 64. A careful examination of such effects is beyond the scope of the present study, but it is clear that the calculated pK shifts caused by Asp 99 are insensitive to drastic changes in the conformation of at least this side chain.

In conclusion, the subtilisin system serves as a very useful test of the linearized Poisson-Boltzmann model for protein electrostatics, and the results are quite promising. On the other hand, it is clear that more tests are necessary in order to explore properly the validity of the model.

The pK Shift of Cys 247 in Rhodanese

The electrostatic potential generated at the thiolate of Cys 247 by the rest of the protein is not the only factor determining the pK of this side chain. The large, positive potential would by itself produce a pK shift of −16 pK units (−22/1.4). A compensating effect probably results from the fact that the sulfur is rather inaccessible to solvent, so its ionized form must be poorly hydrated, and therefore must have a large self-energy relative to a fully solvated thiolate. The Born charging energy[50] may be used to estimate the cost of transferring a thiolate from water to a medium of dielectric constant ~2, representing the protein interior. Treating the thiolate as a sphere of radius

1.97 Å, which is the ionic radius of S^{51} adjusted in accordance with the suggestion of Rashin and Honig,[52] yields a transfer energy of 42 kcal/mol, corresponding to a shift of +30 pK units. The transfer energy in the case of rhodanese's thiolate will be less than this, because the sulfur remains somewhat accessible to solvent and because the dielectric constant of the protein is likely to be somewhat larger than 2, as a consequence of dipolar relaxation during the titration.

Another source of pK change that has been neglected in the present calculations is the transfer energy of the neutral form of the cysteine side chain from water to the protein. It is not clear whether this contribution tends to raise or lower the pK, but it is expected to be small relative to the contributions associated with the charged form.

It should be kept in mind that in the present calculations, polar hydrogens were placed arbitrarily on certain side chains, such as serines (see "Materials and Methods"). This is likely to produce particular problems for the interactions of serines 274 and 181, which are close to the active site cysteine. Further concerns are that the results are quite sensitive to the choice of charge set, and that we have implicitly assumed that hydrogen bonding may be treated as purely electrostatic. Thus, we cannot at this stage calculate pK shifts accurately. We can only break down the various contributions to the pK shift in an approximate way.

α-Helix Dipole Effects in Rhodanese

One of the more striking results presented in this paper is the large effect of α-helices D′ and E′ of rhodanese, which we find stabilize the thiolate by 10–15 kcal/mol. This finding agrees with proposals by Hol[1,31,53] and Wada[33] that the dipole moment of an α-helix can produce substantial electrostatic potentials. One reason for the large effect in the case of rhodanese probably is the rather deep active site cleft. We have found much smaller helix effects in preliminary calculations of helix potentials in a calcium-binding protein in which the ion-binding site juts into the solvent.[54] In addition to this simple solvent exclusion effect, it is possible that the rhodanese cleft also produces electrostatic "focusing" like that found in the active site of Cu,Zn superoxide dismutase.[19]

In general, the ability of α-helices to produce substantial electrostatic potentials probably results in part from the fact that main chain atoms, unlike ionized groups, are often buried in the protein interior where they are less screened by the solvent. Moreover, the electrostatic field produced by a buried dipole tends to be less screened than that of a charge at the same location.[10,55]

Pflugrath and Quiocho have found that the sulfate-binding protein of *Salmonella typhimurium* contains three α-helices with their positive poles near the sulfate.[56] They speculate that the putative stabilizing effect of the helices may be weakened because the sulfate is not centered on any of the helix axes. It is thus worth mentioning that although the thiolate of Cys 247 in rhodanese is not centered on the axis of helix D′, it appears to be strongly influenced by it.

Although helices D′ and E′ do stabilize the catalytically important thiolate form of Cys 247, it may be that their most important function is actually to help bind the enzyme's negatively charged substrates, such as thiocyanate.[32] A large positive potential may be required to accomplish this because bringing the doubly ionized thiocyanate into the narrow active site requires it to be partially desolvated and then brought into contact with the like-charged thiolate of the enzyme. In this context, it should be pointed out that many of the helix dipole functions suggested by Hol and coworkers[1,31] involve anion binding.

An interesting characteristic of ion binding by α-helices is that it appears to contradict conventional wisdom concerning energy of organization. One normally assumes that assembling charges to create a region of high potential involves an electrostatic energy penalty that must be compensated by other, favorable contributions to the energy of protein folding.[57] However, forming an α-helix from random coil is probably electrostatically favorable, since it involves the alignment of dipolar groups. Thus, the same effect that stabilizes the folded form also leads to the net dipole moment, which contributes to ion binding. It seems that here the organization energy is not a cost but a favorable term. A precedent for this situation exists in the case of ferroelectric materials, which exhibit spontaneous polarization in certain temperature ranges.[58] There are two interesting additional parallels between α-helices and ferroelectrics. Uniaxial ferroelectrics always contain dipoles aligned by hydrogen bonding, and ferroelectric crystals tend to form domains, thus minimizing their electrostatic energy.[58] The latter phenomenon is reminiscent of anti-parallel α-helical bundles.

The Range of Electrostatic Interactions

The results presented in this paper suggest that long-range electrostatic interactions may be important in the stabilization of protein structure and in certain protein functions. The general study of charge–charge interactions indicates that two singly charged groups may interact with energies of kT over distances as large as ~25 Å in rhodanese, and ~15 Å in BPTI. These distances are roughly equal to the radii of the proteins, a fact that might serve as a useful rule of thumb. These general results are in accord with the more detailed examination of rhodanese, where 8 histidines more than 8 Å away from the thiolate appear to provide ~10 kT (6 kcal/mol) of stabilization. The experimental results and calculations for subtilisin are also in accord, as charge–charge interactions of ~.5 kT are found at ranges of 12–14 Å. Perhaps surprisingly, neutral dipolar groups

also readily provide several kT of interaction energy over ranges greater than 10 Å, as found for the rhodanese active site. In fact, these groups appear to be much more effective than the ionized groups in creating a positive potential at the thiolate. Unlike ionized groups, however, long-range dipole-charge interactions may require a special organization of the protein, such as an α-helix, to be significant.

One implication of these results is that long range interactions may play important roles in some protein functions. For example, specific binding and the control of the pKs of titratable groups frequently involve small energies, so interactions with remote parts of the protein may play significant roles. The stabilization of protein structure may also involve long-range electrostatic interactions in some cases. In a sense, it is difficult to understand how proteins can perform their functions at all, if the titration of a few distant groups can cause a change in potential of several kT/e^+ in, say, an active site. However, many important phenomena in protein function are sensitive to differences in electrical potential over short distances (i.e., to the electric field) rather than to the potential itself. Since fields fall off considerably faster than potentials as a function of distance, the importance of long-range interactions will be diminished. For example, it is unlikely that long-range potentials have a significant effect on the movement of a proton over a distance of ~ 1 Å in the charge relay system of a serine protease, even though the same potentials might alter the activation energy of forming a charged intermediate.

An additional consequence of these results is that caution should be used when applying cutoff radii to nonbonded interactions in molecular mechanics simulations. However, as noted above, it may be reasonable to use smaller cutoff radii in cases in which dynamics, rather than energies, are of interest, as the former depend only on fields, while the latter depend on potentials as well.

Validity of Simple Electrostatic Models

Tanford-Kirkwood theory

The straightforward application of Tanford-Kirkwood theory with charges placed at realistic depths gives reasonable overall agreement with the detailed Poisson-Boltzmann results, based on examination of the general calculations of charge–charge interactions, and on the rhodanese active site potential calculations. Tanford-Kirkwood theory can thus serve as a convenient approximation to the full Poisson-Boltzmann solutions, at least in the case of globular proteins. On the other hand, the general calculations show that this model tends to overestimate weak interactions, a conclusion borne out by the subtilisin pK shift results. Artificially moving surface charges slightly closer to the surface can serve as a crude and probably justifiable fix for this problem. However, the adjustments used in the Modified Tanford-Kirkwood theory (see "Results") tend to overcompensate for the problem, as indicated by the excessively small pK shifts obtained for subtilisin.

Distance-dependent dielectric model

A number of calculations presented in this paper suggest that the distance-dependent dielectric constant $\epsilon = R$ yields excessively large electrostatic interactions. For the surface charges in subtilisin, $\epsilon = R$ yields interactions that are at least three times too strong (Tables I, II), and it predicts an active site potential in rhodanese that is nearly twice as large as what is given by the detailed Poisson-Boltzmann calculation (although certain contributions are in better agreement than this) (see Table III). In the general examination of charge–charge interactions for rhodanese and BPTI, $\epsilon = R$ overestimates by factors of 2 to 30 potentials that, according to the detailed Poisson-Boltzmann solutions, should be between 0 and 1 kcal/(mol-e^+). The severity of the overestimation depends on the ionic strength. Stronger potentials may or may not be overestimated, depending on the case. The tendency to overestimate is, not surprisingly, greater in the smaller protein.

The finding that $\epsilon = R$ underscreens electrostatic interactions in a small protein is in accord with a recent observation made by Whitlow and Teeter.[59] These authors performed energy minimizations on the protein crambin using a number of different electrostatic energy terms. Minimizations that included more screening than was provided by $\epsilon = R$ yielded better agreement with the crystallographically determined structure. The best screening function they tried was $\epsilon = 4R$. It is worth noting that we would predict even greater overscreening by $\epsilon = R$ for crambin than for BPTI, since crambin is a smaller protein (see "Results"). Whitlow and Teeter suggest further that incorporating additional screening for charges near the solvent might improve their results. Such a correction would also follow from the Poisson-Boltzmann model.

In conclusion, the distance-dependent dielectric model does not appear to be a particularly realistic way of treating solvent screening in molecular simulations. A method of increasing screening for charges near the protein surface might represent a desirable improvement. A simpler form of improvement might be to employ a dielectric function whose magnitude would depend on the size of the protein under study, and possibly the ionic strength of the solvent.

Coulomb's law and Debye-Huckel theory

The excessively large potentials found using Coulomb's law with $\epsilon = 2$ in calculating the rhodanese active site potential illustrate the importance of accounting for solving screening in quantum chemical and molecular mechanics calculations. Debye-Huckel theory might constitute an improvement since it could, in principle, represent a convenient ionic

strength correction for protein electrostatics. However, it yields potentials that are much too small, because it neglects both the low protein dielectric constant and the protein's ion-excluding volume.

ACKNOWLEDGMENTS

We are grateful to Drs. Kim Sharp and Hillary Gilson for their helpful comments and suggestions, to Dr. Philippe Youkharibache for his assistance with molecular modeling, and to Dr. Moshe Eisenberg for his helpful suggestions concerning the text. This work was supported by a grant (GM-30518) from the National Institutes of Health.

NOTE ADDED IN PROOF

The empirical ϵ (r) curve I of Mehler and Eichele (Biochemistry 23:3887–3891, 1984) yields a pK shift of .33 at low ionic strength for Asp 99 in subtilisin in excellent agreement with the experimental result. The empirical ϵ (r) function of Warshel et al. (Proc. Natl. Acad. Sci. 81:4585–4589, 1984) yields .36 and .45 for the low ionic strength pK shifts of Asp 99 and Glu 156, respectively. Reference 28 incorrectly reported .51 and .61 for the shifts provided by this function; the latter values correspond to free energy changes, not pK shifts.

REFERENCES

1. Hol, W.G.J. The role of the α-helix dipole in protein function and structure. Prog. Biophys. Mol. Biol. 45:149–195, 1985.
2. Honig, B., Hubbell, W., Flewelling, R. Electrostatic interactions in membranes and proteins. Annu. Rev. Biophys. Chem. 15:163–193, 1986.
3. Matthew, J.B. Electrostatic effects in proteins. Annu. Rev. Biophys. Biophys. Chem. 14:387–417, 1985.
4. Warshel, A., Russell, S.T. Calculation of electrostatic interactions in biological systems and in solution. Q. Rev. Biophys. 17:283–422, 1985.
5. Kakitani, H., Kakitani, T., Rodman, H., Honig, B. On the mechanism of wavelength regulation in visual pigments. Photochem. Photobiol. 41:471–479, 1985.
6. Nakanishi, K., Balogh-Nair, V., Arnaboldi, M., Tsujimoto K., Honig, B. An external point-charge model for bacteriorhodopsin to account for its purple color. J. Am. Chem. Soc. 102:7945–7947, 1980.
7. Perutz, M.F. Electrostatic effects in proteins. Science 201:1187–1191, 1978.
8. Neumann, M. The dielectric constant of water. Computer simulations with the MCY potential. J. Chem. Phys. 82:5663–5672, 1985.
9. Steinhauser, O. On the orientational structure and dielectric properties of water. A comparison of ST2 and MCY potential. Ber. Bunsenges. Phys. Chem. 87:128–142, 1983.
10. Gilson, M.K., Rashin, A., Fine, R., Honig, B. On the calculation of electrostatic interactions in proteins. J. Mol. Biol. 183:503–516, 1985.
11. Gilson, M.K., Honig, B.H. The dielectric constant of a folded protein. Biopolymers 25:2097–2119, 1986.
12. Imoto, T. Electrostatic free energy of lysozyme. Biophys. J. 44:293–298, 1983.
13. Orttung, W. Proton binding and dipole moment of hemoglobin. Refined calculations. Biochemistry 9:2394–2402, 1970.
14. Shire, S.J., Hanania, G.I.H., Gurd, F.R.N. Electrostatic effects in myoglobin. Hydrogen ion equilibria in sperm whale ferrimyoglobin. Biochemistry 13:2967–2974, 1974.
15. Tanford, C., Kirkwood, J.G. Theory of protein titration curves. I. General equations for impenetrable spheres. J. Am. Chem. Soc. 79:5333–5339, 1957.
16. Tanford, C., Roxby, R. Interpretation of protein titration curves. Application to lysozyme. Biochemistry 11:2192–2198, 1972.
17. Kirkwood, J.G. Theory of solutions of molecules containing widely separated charges with special applications to zwitterions. J. Chem. Phys. 2:351–361, 1934.
18. Gilson, M.K., Sharp, K.A., Honig, B.H. Calculating electrostatic interactions in bio-molecules: method and error assessment. J. Comput. Chem. (in press).
19. Klapper, I. Hagstrom, R., Fine, R., Sharp, K., Honig, B. Focusing of electric fields in the active site of Cu-Zn superoxide dismutase: Effects of ionic strength and amino-acid modification. Proteins 1:47–59, 1986.
20. Rogers, N.K., Sternberg, M.J.E. Electrostatic interactions in globular proteins. J. Mol. Biol. 174:527–542, 1984.
21. Warwicker, J., Watson, H.C. Calculation of electric potential in the active site cleft due to α-helix dipoles. J. Mol. Biol. 157:671–679, 1982.
22. Zauhar, R.J., Morgan, R.S. A new method of computing the macromolecular electric potential. J. Mol. Biol. 186:815–820, 1985.
23. Warwicker, J., Ollis, D., Richards, F.M., Steitz, T.A. Electrostatic field of the large fragment of *Escherichia coli* DNA polymerase I. J. Mol. Biol. 186:645–649, 1985.
24. Sharp, K., Fine, R., Honig, B. Computer simulations of the diffusion of a substrate to an active site of an enzyme. Science 236:1460–1463, 1987.
25. Sharp, K., Fine, R., Schulten, K., Honig, B. Brownian dynamics simulation of diffusion to irregular bodies. J. Phys. Chem. 91:3624–3631, 1987.
26. Warwicker, J. Continuum dielectric modelling of the protein-solvent system, and calculation of the long-range electrostatic field of the enzyme phosphoglycerate mutase. J. Theor. Biol. 121:199–210, 1986.
27. Rogers, N.K., Moore, G.R., Sternberg, M.J.E. Electrostatic interactions in globular proteins: calculations of the pH dependence of the redox potential of cytochrome c551. J. Mol. Biol. 182:613–616, 1985.
28. Gilson, M.K., Honig, B.H. Calculation of electrostatic potentials in an enzyme active site. Nature 330:84, 1987.
29. Russell, A.J., Thomas, P.G., Fersht, A.R. Electrostatic effects on modification of charged groups in the active site cleft of subtilisin by protein engineering. J. Mol. Biol. 193:803–813, 1987.
30. Thomas, P.G., Russell, A.J., Fersht, A.R. Tailoring the pH dependence of enzyme catalysis using protein engineering. Nature 318:375–376, 1985.
31. Hol, W.G.J., van Duijnen, P.T., Berendsen, H.J.C. The α-helix dipole and the properties of proteins. Nature 273:443–446, 1978.
32. Ploegman, J.H., Drenth, G. Kalk, K.H., Hol, W.G.J. The structure of bovine liver rhodanese II. The active site in the sulfur-substituted and the sulfur free enzyme. J. Mol. Biol. 127:149–162, 1979.
33. Wada, A. The α-helix as an electric macro-dipole. Adv. Biophys. 9:1–63, 1976.
34. Weiner, S.J., Kollmann, P.A., Case, D.A., Singh, U.C., Ghio, C., Alagona, G., Profeta, S. Jr., Weiner, P. A new force field for molecular mechanical simulation of nucleic acids and proteins. J. Am. Chem. Soc. 106:765–784, 1984.
35. Brooks, B.R., Bruccoleri, R.E., Olafson, B.D., States, D.J., Swaminathan, S., Karplus, M. CHARMM: A Program for macromolecular energy, minimization, and dynamics calculations. J. Comput. Chem. 4:187–217, 1983.
36. Richards, F.M. Areas, volumes, packing, and protein structure. Ann. Rev. Biophys. Bioeng. 6:151–176, 1977.
37. McCammon, J.A., Wolynes, P.G., Karplus, M. Biochemistry 18:927–942, 1979.
38. Lee, B., Richards, F.M. The interpretation of protein structures: estimation of static accessibility. J. Mol. Biol. 55:379–400, 1971.
39. Bockris, J.O'M., Reddy, A.K.N. "Modern Electrochemistry" V. 1. New York: Plenum 1977.
40. Bernstein, F.C., Koetzle, T.F., Williams, G.J.B., Meyer, E.F. Jr., Brice, M.D., Rodgers, J.R., Kennard, O., Shimanouchi, T., Tasumi, M.J. The protein data bank: A computer-based archival file for molecular structures. J. Mol. Biol. 112:535–542, 1977.
41. Ploegman, J.H., Drent, G., Kalk, K.H., Hol, W.G.J. Struc-

ture of bovine liver rhodanese. I. Structure determination at 2.5 Å Resolution and a comparison of the conformation and sequence of its two domains. J. Mol. Biol. 123:557–594, 1978.
42. Marquart, M., Walter, J., Diesenhofer, J., Bode, W., Huber, R. The geometry of the reactive site and of the peptide groups in trypsin, trypsinogen and its complexes with inhibitors. Acta. Cryst., Sect. B 39:480, 1983.
43. Alden, R.A., Birktoft, J.J. Kraut, J., Robertus, J.D., Wright, C.S. Atomic coordinates for subtilisin BPN (or Novo). Biochem. Biophys. Res. Commun. 45:337, 1971.
44. Connolly, M.L. Solvent-accessible surfaces of proteins and nucleic acids. Science 221:709, 1983.
45. Katz, L., Levinthal, C. Interactive computer graphics and representation of complex biological structures. Annu. Rev. Biophys. Bioeng. 1:465–504, 1972.
46. Dr. Alan Fersht, personal communication.
47. Finkel'shtein, A.V. Electrostatic interactions of charged groups in an aqueous medium and their effect on the formation of polypeptide chain secondary structure. Mol. Biol. 11:627–634, 1978.
48. Troll, M., Roitman, D., Conrad, J., Zimm, B.H. Electrostatic interactions between ions and DNA estimated with an electrolyte tank. Macromolecules 19:1186–1194, 1986.
49. Berry, R.S., Rice, S.A., Ross, J. "Physical Chemistry." New York: John Wiley & Sons, 1980.
50. Born, M. Volumes and heats of hydration of ions. Z. Physik. 1:45–48, 1920.
51. "CRC Handbook of Chemistry and Physics", Weast, R.C. (ed.) 56th ed. OH: CRC Press, Cleveland, 1975.
52. Rashin, A.A., Honig, B. Reevaluation of the Born model of ion hydration. J. Chem. Phys. 89:5588–5593, 1985.
53. van Duijnen, P. Th., Thole, B. Th., Hol, W.G.J. On the role of the active site helix in papain, an ab initio molecular orbital study. Biophys. Chem. 9:273–280, 1979.
54. Jean-Charles, A., Gilson, M.K., Sharp, K.A., Honig, B.H., unpublished results.
55. Gilson, M.K., Honig, B.H., unpublished results.
56. Pflugrath, J.W., Quiocho, F.A. Sulphate sequestered in the sulphate-binding protein of Salmonella typhimurium is bound solely by hydrogen bonds. Nature 314:257–260, 1985.
57. Fersht, A. "Enzyme Structure and Mechanism." New York: Freeman, 1985.
58. Anderson, J.C., "Dielectrics." London: Chapman and Hall, 1966.
59. Whitlow, M., Teeter, M.M. An empirical examination of potential energy minimization using the well-determined structure of the protein crambin. J. Am. Chem. Soc. 108:7163–7172, 1986.
60. Sternberg, M.J.E., Hayes, F.R.F., Russell, A.J., Thomas, P.G., Fersht, A.R. Prediction of electrostatic effects of engineering of protein charges. Nature 330:86–88, 1987.